RSC Advances

ROYAL SOCIETY OF CHEMISTRY

www.rsc.org/advances

Synthesis of SiO_2 Coated Zero-valent Iron/Palladium Bimetallic Nanoparticles and Application in a Nano-biological Combined System for 2,2'4,4'-Tetrabromodiphenyl ether Degradation

Yuancai Lv[a,1], Zhuyu Niu[b,2], Yuancai Chen[a,b*], Yongyou Hu[a,b,3]

[a] State Key Laboratory of Pulp and Paper Engineering, College of Light Industry and Food Science, South China University of Technology, Guangzhou, 510640, China

[b] Ministry of Education Key Laboratory of Pollution Control and Ecological Remediation for Industrial Agglomeration Area, College of Environment and Energy, South China University of Technology, Guangzhou, 510006, China

[*]Corresponding Author's E-mail: chenyc@scut.edu.cn; Phone: +86 13672458060; Address: State Key Laboratory of Pulp and Paper Engineering, South China University of Technology, No.281 Wushan Road, Tianhe District, Guangzhou, Guangdong, 510640, P. R. CHINA

[1] Email: donkey1204@hotmail.com, [2] Email: niuzhuyu11@163.com,

[3] Email: ppyyhu@scut.edu.cn

Abstract

Polybrominated diphenyl ethers (PBDEs) are emerging persistent organic pollutants and the degradation of PBDEs is still a significant challenge owing to their extreme persistence and toxicity. In this study, the remediation of 2,2'4,4'-Tetrabromodiphenyl ether (BDE47) was investigated by employing a nano-biological combined system with SiO_2-coated zero-valent iron/palladium bimetallic nanoparticles (SiO_2-nZVI/Pd) as reductant and *Pseudomonas putida* as biocatalyst. The SiO_2-nZVI/Pd exhibited much lower toxicity to *P. putida* strain and higher reactivity on debromination than nZVI/Pd. The strain could grow well when the dosage was up to 1.0 g L^{-1}. During the combined process, BDE47 (5 mg L^{-1}) was completely debrominated to diphenyl ether (DE) within 2 h by SiO_2-nZVI/Pd (1.0 g

L^{-1}) and then DE was completely degraded by *P. putida* after 4 days in the sequential aerobic biodegradation. All the possible intermediates in the whole process were identified by ultra performance liquid chromatography (UPLC) and gas chromatography-mass spectrometer (GC-MS) analyses. The detect of BDE17, BDE7, BDE1 and DE indicated that rapidly stepwise debromination preferentially occurred at *para* positions in anaerobic stage. Moreover, during aerobic biodegradation by *P. putida*, a number of phenolic compounds, such as phenol, catechol and hydroquinone were generated via ring opening by dioxygenation and further mineralized through the tricarboxylic acid cycle (TCA). Importantly, this combined process achieved the rapidly mineralization of PBDEs and avoided the generation of some highly toxic products like bromphenols and HO-PBDEs, which might have a promising application prospects in the remediation of halogenated POPs.

Key words

Polybrominated diphenyl ethers (PBDEs), Nano-biological combined process, Reductive debromination, Nanoscale zero valent iron, *Pseudomonas putida*

1 Introduction

As one kind effective and economical flame retardant, polybrominated diphenyl ethers (PBDEs) have been widely used in a variety of industrial products.[1] At present, PBDEs have been detected frequently in air, soil, sediment and sewage sludge samples, even in biological samples.[1-4] Among the PBDEs congeners, 2,2',4,4'-tetrabromodiphenyl ether (BDE47) is the most widely distributed congener in environment and organism samples[3,5] and has some serious health side-effects such as thyroid hormone disruption, neurotoxicity and abnormal behaviors.[6] Thus, it is highly urgent to explore effective strategies to deal with BDE47.

Biodegradation exhibited environmentally friendly sights for persistent organic

pollutants (POPs) remediation and was deemed as an effective, economic and safe way. Meanwhile, a considerable number of microorganisms have been reported to be able to degrade PBDEs.[3,7,8] However, biodegradation of PBDEs often needed a rather long operation time and generated some more toxic products such as bromphenols[9], HO-PBDEs[8] and MeO-PBDEs[10].

Recently, owing to its high reactivity, nano technology has become an efficient treatment in the elimination of contaminants.[11,12] Based on this, the nano-biological integrated system has attracted great attention and is considered as a potential strategy for the remediation of halogenated POPs[13-15]. In which, as an effective pretreatment process. nZVI and its composite materials could rapidly and greatly reduce the resistance of the contaminants and greatly improved the efficiency in biological process. Murugesan et al.[13] found that an integrated redox process consisting of nZVI/Pd mediated reductive dehalogenation followed by oxidative degradation by *sphingomonas sp*. PH-07 was an efficient strategy for complete degradation of TCS. Similarly, Kim et al.[16] also found the combined system of nZVI and aerobic biodegradation could transform BDE-209 into small molecular substances. According to Shih et al.'s[17] study, it could immensely improve the degradation of deca-BDE when combining ZVI with the anaerobic sludge.

However, two problems limited the application of nZVI/biological process. Due to the strong magnetic effects between the nanoparticles, a severe agglomeration occurred, which greatly decreased the activities of nZVI or nZVI composite materials.[18-20] On the other hand, it has been proved that nZVI particles could greatly inactivate the bacterial cells through physical coating, membrane disruption and oxidative stress.[21-23] The strong antibacterial activities of nZVI or nZVI/Pd particles significantly limited application. According to the previous studies, some attempts

have verified that surface coated nZVI particles with polymer and natural organic matter (NOM) or sodium-oleate decreased the toxicity of nZVI particles to *E. coli* when compared with non-coated nZVI particles,[24,25] which was attributed to the fact that the coating prevented the adhesion of nZVI particles onto cell membrane.

In this study, a nano-biological hybrid process was employed to completely mineralize BDE47 with SiO_2-nZVI/Pd particles and *Pseudomonas putida* strain. In order to improve the debromination efficiency and reduce the toxicity to *P. putida* strain, the nZVI/Pd particles were coated with SiO_2 film by using tetraethyl orthosilicate (TEOS) as silicon source and their toxic effects on *P. putida* and reactivity were both evaluated. BDE47 was firstly completely debrominated to DE by SiO_2-nZVI/Pd particles under anaerobic condition, making the effluent much easier for subsequent biological mineralization. Then DE was subsequently treated with *P. putida* strain. Here, the degradation kinetics of the reduction debromination was examined. The intermediates during the whole process were monitored and the degradation pathways of PBDEs by this treatment were explored.

2 Material and methods

2.1 Materials

2,2'4,4'-Tetrabromodiphenyl ether (BDE47, 99%) and Diphenyl ether (DE, 99%) were purchased from J&K Scientific Ltd. and Sigma-Aldrich, respectively. BDE-1, BDE-3, BDE-7, BDE-15, BDE-17, BDE-28 and BDE-47 at 50 μg mL^{-1} in isooctane were from AccuStandard. HPLC grade methanol and dichloromethane were separately supplied by Merck (Germany) and CNW (Germany). $FeSO_4 \cdot 7H_2O$ (99%), NaBH4 (98%) and ethyl alcohol (99.7%) were purchased from Aladdin (Shanghai, China). Deionized Water was prepared by the Milli-Q water purification system (Millipore). The strain, *Pseudomonas putida*, was isolated from the sludge of pulping

wastewater and kept in our laboratory. Minimal salt medium (MSM) and phosphate buffer (pH 7.00) were prepared by the method reported previously[26]. Before use, the MSM and phosphate buffer were previously sterilized in an autoclave at 121 ºC for 30 min.

2.2 Synthesis and characterization of SiO_2-coated zero-valent iron/palladium bimetallic nanoparticles

Synthesis of SiO_2-coated zero-valent iron/palladium bimetallic nanoparticles (SiO_2-nZVI/Pd) was carried by reducing $FeSO_4 \cdot 7H_2O$ with $NaBH_4$ under nitrogen atmosphere. The detailed information could be seen in supporting information.

The morphology of SiO_2-nZVI/Pd particles was observed with transmission electron microscopy (TEM, JEM 2100F, Japan). The N_2 Brunnaer-Emmett-Teller (BET) specific surface areas of the particles were measured by ASAP 2020. X-ray diffraction (XRD) spectra were obtained using Cu *Ka* radiation at 40 kV and 40 mA (MAC Science Co., M18XHF).

2.3 Toxicity of nZVI/Pd and SiO_2-nZVI/Pd particles to *P. putida*

The toxicity evaluation was based on the effects of nZVI/Pd and SiO_2-nZVI/Pd particles on the growth and inactivation of *P. putida* strain. Experiments were conducted using different amounts of nZVI/Pd and SiO_2-nZVI/Pd particles (0, 0.5 and 1.0 g L^{-1}) in 250 mL Erlenmeyer flasks containing 50 mL of sterilized MSM medium. The initial cell concentration was about $2.0\pm0.6\times10^7$ CFU mL^{-1} (about 0.025 of OD_{600}). Flasks were incubated in a shaking incubator at 200 rpm at 30 ºC. For growth test, 2 g L^{-1} of glucose was added as carbon source while no glucose was supplied in inactivation test. At the sampling points, 100 μL of culture was aseptically drawn out and plated onto nutrient agar media (incubated at 37 °C for 24 h) after the proper dilution to monitor the number of *P. putida* cells and evaluate the toxic effect of

particles. To find out whether nZVI/Pd and SiO_2-nZVI/Pd particles affect cell membrane and morphology of *P. putida* cells, TEM analysis was performed. The samples for TEM analysis were prepared as followed standard protocol (see supporting information).

2.5 Sequential aerobic treatment followed anaerobic debromination

After anaerobic debromination process, all the rubber caps were removed. Then 2.0 mL of prepared resting cells (seen in supporting information) of *P. putida* in MSM were poured into the bottles to make a cell number of about $1.5\pm0.3\times10^8$ CFU mL^{-1}. All test bottles were incubated for further 4 days under identical conditions, while the bottles were capped with trilaminar sterile gauze to supply fresh air. The test bottles that contained debrominated products without resting cells were set as controls. At preselected time intervals, three bottles were drew out and the samples were analyzed after extraction.

2.4 Anaerobic debromination by SiO_2-nZVI/Pd particles

Anaerobic debromination of BDE-47 was conducted under nitrogen atmosphere in serum bottles (100 mL). 200 μL of BDE-47 stock solution (dissolved in toluene, 1 000 mg L^{-1}) was added to the bottle. After gentle vaporization of the solvent through N_2, 19.0 mL deoxygenated MSM and 1.0 mL SiO_2-nZVI/Pd slurry were separately poured into the bottle in a glove box (LM1000S, Dellix Industy Co. LTD, China). N_2 was kept in the headspace of the test tube before sealing the Teflon coated rubber cap with aluminium crimp. These bottles were incubated in a shaking incubator at 200 rpm at 30 ºC. The controls were operated in same process but without SiO_2-nZVI/Pd. At each sampling point, three bottles were collected and analyzed after extraction (see supporting information).

2.6 Analytical methods

BDE47 and DE concentrations were detected by ultra performance liquid chromatography (UPLC, Waters ACQUITY UPLC system, America). The intermediates and products during the whole treatment were identified by Thermo Trace GC Ultra instrument coupled to a Thermo DSQ II mass spectrometer (Thermo Electron Corporation, Waltham, USA). The concentration of Bromide ions (Br^-) were determined by an ion-chromatography system (ICS-90, Dionex). The detailed information could be seen in supplementary information.

TOC was determined by LiquiTOC trace (Elementar, Germany). Before determination, all the samples were with 0.22 μm glass fiber filters.

2.7 Statistical analysis

All experiments were performed in triplicate and the data were expressed as mean ± standard deviation. The statistical analyses were performed with one-way analysis of variance (ANOVA) using Minitab 16 Software. A multiple comparison Tukey test was applied to assay the differences among treatments.

3 Results and discussion

3.1 Particle Characterization

Fig.1 and Fig.S1 showed TEM images and size distribution of SiO_2-nZVI/Pd and nZVI/Pd particles. Similar to the previous reports,[18,19] the magnetic effects between the nanoparticles caused server agglomeration of nZVI/Pd particles without SiO_2 (Fig.S1a and b). However, once nZVI/Pd particles were coated with a transparent and corrugated SiO_2 film, it can be clearly observed an evident decrease on the aggregation between nZVI/Pd particles and the synthetized nZVI/Pd particles formed linear chains in space (Fig.1a-d). The particle size of nZVI/Pd without SiO_2 was mainly (92.1%, Fig.S1c) in the range of 20-40 nm while the main particle size (75.0%, Fig.1e) increased to 30-50 nm when coated with SiO_2. All the results indicated that

the coated SiO_2 film on nZVI/Pd surface prevented the agglomeration of nZVI/Pd particles and slightly increased their sizes.

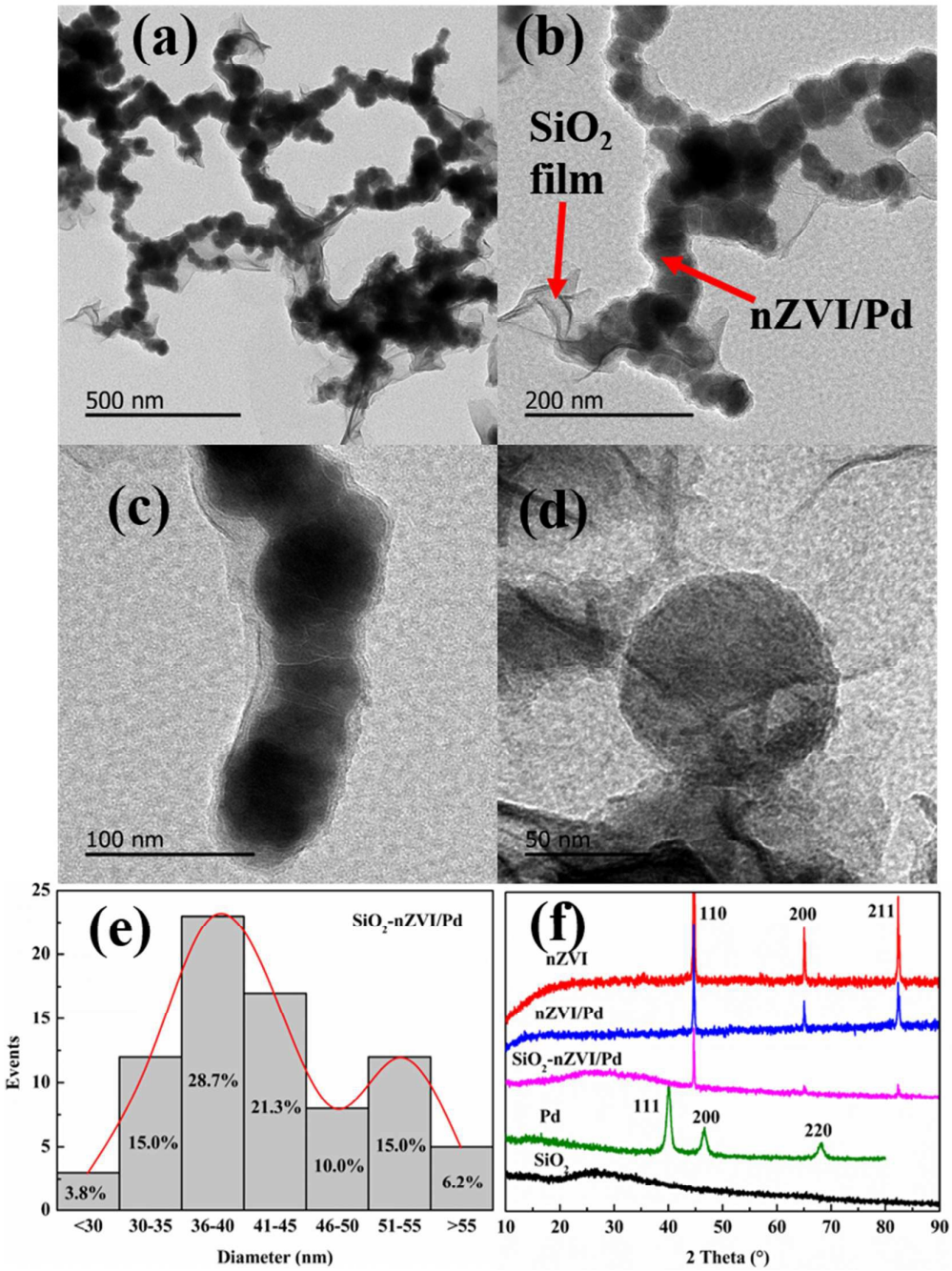

Fig.1 TEM images (a-d) and size distribution (e) of SiO_2-nZVI/Pd and XRD (f) spectra of SiO_2-nZVI/Pd, nZVI/Pd, nZVI, Pd and SiO_2.

Fig.1f exhibited the XRD patterns of SiO_2, Pd, fresh synthesized nZVI/Pd, nZVI

and SiO_2-nZVI/Pd, respectively. In the pattern of fresh synthesized SiO_2-nZVI/Pd, it clearly depicted a weak characteristic diffraction peak of SiO_2, located at $2\theta = 27.36°$, and three characteristic diffraction peaks appeared at $2\theta = 44.69°$, 65.02° and 82.35°, which were in accordance with nZVI/Pd and nZVI. The three peaks can be indexed as the (110), (200) and (211) plane of α-Fe^0 (JCPDS card no. 06-0696). However, due to the low dosage, no characteristic diffraction peaks ($2\theta = 39.8°$, 46.2° and 67.8°) of palladium were observed, which was similar with Zhang et al.'s study[19]. Furthermore, Inductively Coupled Plasma Optical Emission Spectrometry (ICP-OES) was employed to determine the percentage of Fe, Pd and Si in SiO_2-nZVI-Pd. The results showed that the percentages of Fe, Pd and Si were 87.61%, 0.26% and 5.78%, respectively, indicating the successful synthesis of SiO_2-coated zero-valent iron/palladium bimetallic nanoparticles.

The BET specific surface area of the synthetized nZVI/Pd particles was 32.68 m^2 g^{-1}, which agreed with data reported in studies that employed similar synthesis methods.[27] Similarly, the BET specific surface areas of SiO_2-nZVI/Pd and SiO_2 after vacuum drying were 111.76 and 268.54 m^2 g^{-1}, respectively. This could be ascribed to two reasons. On one hand, which was more important, the presence of corrugated SiO_2 film on the surface of nZVI/Pd greatly expand the BET specific surface area of nZVI/Pd. On the other hand, the reducing of agglomeration also could partly improve the particles' BET specific surface area.

3.2 Toxicity and reactivity of SiO_2-nZVI/Pd and nZVI/Pd

3.2.1 Toxicity of SiO_2-nZVI/Pd and nZVI/Pd to *P. putida* cells

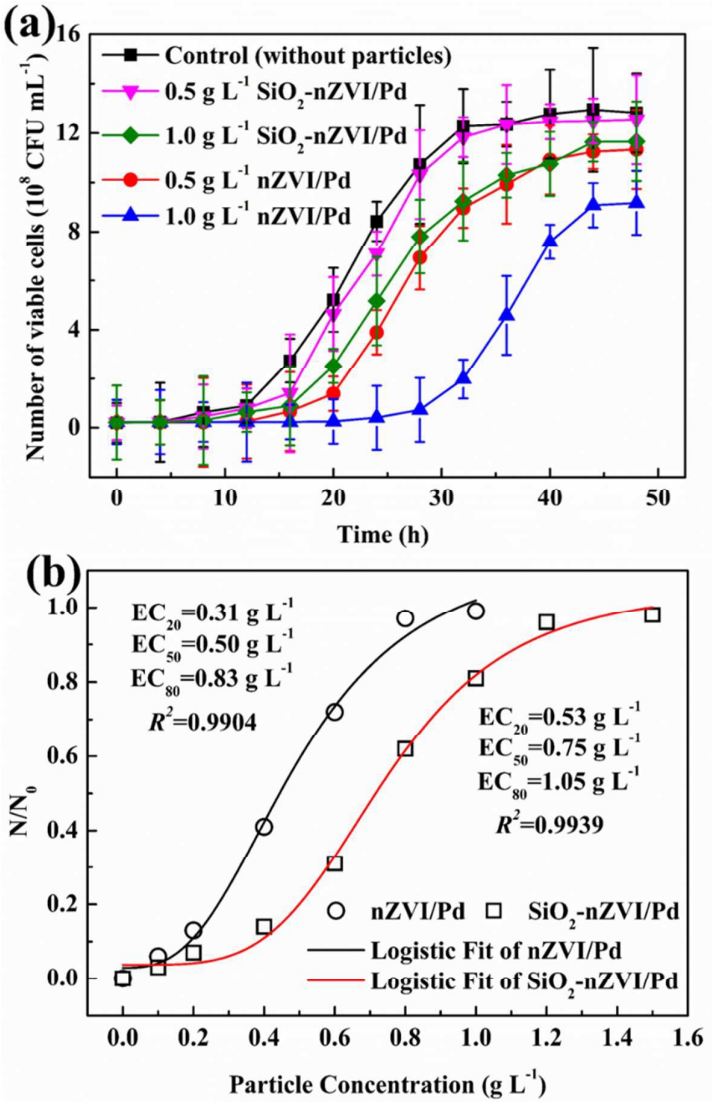

206

207 Fig.2 Effect of nZVI/Pd and SiO_2-nZVI/Pd nanoparticles on the growth (a) and

208 inactivation (b) of *P. putida* in MSM medium. Initial cell concentration: $2.0\pm0.6\times10^7$

209 CFU mL^{-1} and initial pH: 7.00.

210 It was well known that the nanoparticles were toxic to bacterial cells.[21-23] Thus, it

211 was important to evaluate the toxicity of the nanoparticles to the cells when a

212 nano-bio treatment involving nanoparticles and bacteria was employed for efficient

213 degradation of pollutants. Here, in order to evaluate the antibacterial activity of

214 SiO_2-nZVI/Pd and nZVI/Pd, the growth and inactivation of *P. putida* cells under

different dosage of nanoparticles (with ranges from 0.0 to 1.0 g L^{-1}) was conducted (Fig.2). Considering the interference of the dispersed nZVI particles on the accurate spectrophotometric measurement of the cell suspensions, the cell growth was assessed with colony forming unit (CFU) counting. As shown in Fig.2a, *P. putida* strain was able to grow well when the dosage of nZVI/Pd was 0.5 g L^{-1} in MSM whereas bacterial growth was drastically inhibited with high nZVI/Pd amount (1.0 g L^{-1}). However, the *P. putida* strain could still grow well even SiO_2-nZVI/Pd dosage was up to 1.0 g L^{-1}, suggesting that SiO_2-nZVI/Pd was less toxic than nZVI/Pd. Compared with control, the lag phases of *P. putida* cell were 8 h (0.5 g L^{-1} of SiO_2-nZVI/Pd), 16 h (1.0 g L^{-1} of SiO_2-nZVI/Pd), 12 h (0.5 g L^{-1} of nZVI/Pd) and 24 h (1.0 g L^{-1} of nZVI/Pd), respectively, which were longer than that of control culture (4 h), indicating the nanoparticles prolonged the exponential phase of cell growth.

To evaluate the toxicity of nZVI/Pd in quantitative manner, Logistic model[28] was employed to obtain the relative parameters. The high R^2 values (0.9904 and 0.9939, Fig.2b) suggested Logistic model could well describe the effects of various particle concentrations on the inactivation of *P. putida*. The EC_{20}, EC_{50} and EC_{80} of SiO_2-nZVI/Pd were 0.53, 0.75 and 1.05 g L^{-1}, respectively, which was 1~2 times larger than that of nZVI/Pd (0.31, 0.50 and 0.83 g L^{-1}). The results indicated that the coating of SiO_2 on nZVI/Pd could greatly reduce the toxicity to *P. putida* cells.

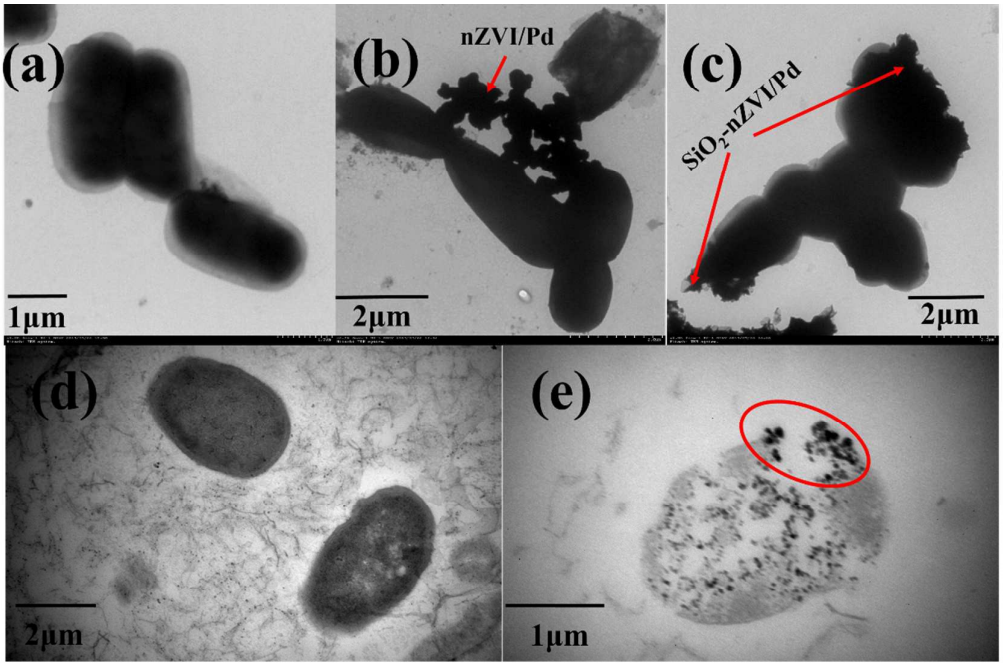

Fig.3 TEM images of *P. putida* cells (a), nZVI/Pd treated cells (b) and SiO_2-nZVI/Pd treated cells (c) and the biological slices of *P. putida* cells (d) and nZVI/Pd treated cells (e). Initial cell concentration: $2.0\pm0.6\times10^7$ CFU mL^{-1}, nZVI/Pd dosage: 0.5 g L^{-1} and SiO_2-nZVI/Pd dosage: 1.0 g L^{-1}.

To check the effects of nZVI/Pd and SiO_2-nZVI/Pd on morphology of *P. putida* cells, both the control and particles treated cells were analyzed by TEM (Fig.3). Compared with untreated cells (Fig.3a), the TEM images (Fig.3b and c) clearly revealed a large amount of nZVI/Pd particles adhered to the surface of cells once nZVI/Pd particles were added. As shown in Fig.3b, some cells were broken while no ruptured cells were observed in Fig.3c, suggesting the coating of SiO_2 greatly decreased the toxicity of nZVI/Pd particales. As reported in previous studies, surface coated nZVI with polymer or NOM prevented the adhesion of nZVI particle onto cell membrane, leading to the decrease of toxicity of nZVI to *E. coli*.[24] Similarly, the toxicity of nZVI particles greatly declined when combined with sodium-oleate.[25] Furthermore, the TEM images of biological slices (Fig.3e and f) clearly exhibited the

rupture of the cell membrane caused by adhered nZVI/Pd particles, leading to the inactivation of cells. Kim et al.[23] also observed severe damages caused by nZVI particles to the cell membranes of *Escherichia coli*.

Although an initial retardation in growth were observed in the presence of SiO_2-nZVI/Pd, the cell number was almost equal to the control as incubation progressed (Fig.2), indicating that *P. putida* strain could tolerate SiO_2-nZVI/Pd with the range of 0-1.0 g L^{-1}. Therefore, SiO_2-nZVI/Pd could be employed for degradation of PBDEs in the nano-bio treatment process.

3.2.2 Ractivity of SiO_2-nZVI/Pd and nZVI/Pd on BDE47 remediation

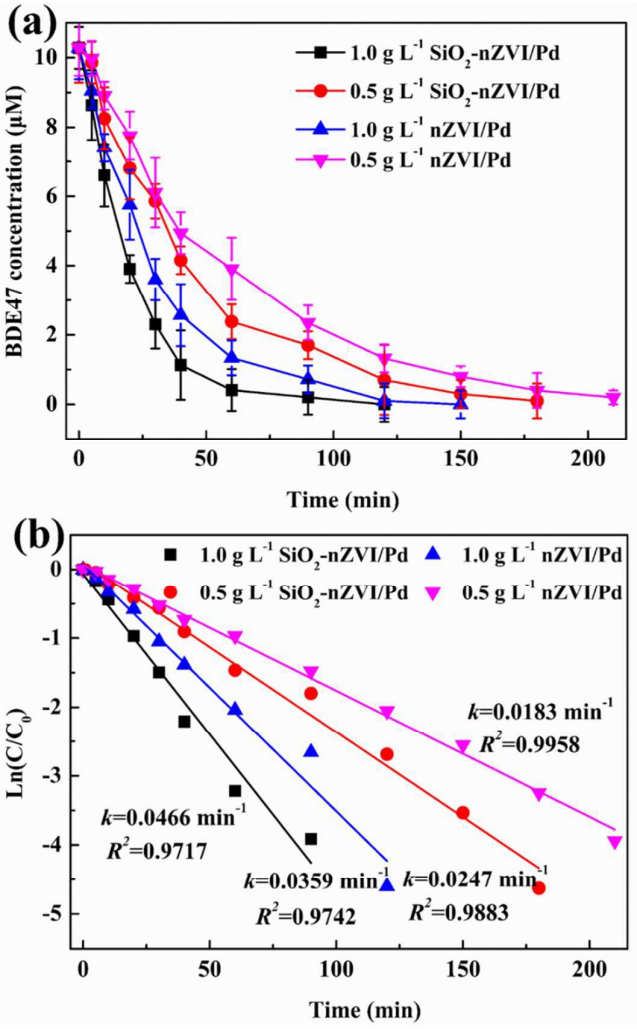

Fig.4 Effects of particle dosage on degradation of BDE47

Although SiO_2 played an important role in reducing the biotoxicity, whether it could enhance PBDEs degradation was indistinct. Fig.4 illustrated the degradation efficiencies and rates of BDE47 by SiO_2-nZVI/Pd and nZVI/Pd with different dosages. As shown in Fig.4a, both SiO_2-nZVI/Pd and nZVI/Pd exhibited excellent elimination of BDE47. It took 120 and 180 min to completely degrade BDE47 for 1.0 and 0.5 g L^{-1} of SiO_2-nZVI/Pd, which were lower than that of nZVI/Pd (150 and >210 min for 1.0 and 0.5 g L^{-1}). Meanwhile, the degradation of BDE47 obeyed the pseudo-first-order model with 0.0466 (1.0 g L^{-1}) and 0.0247 min^{-1} (0.5 g L^{-1}) of rate constant for SiO_2-nZVI/Pd, which were 1.3~1.5 times larger than those (0.0359 and 0.0183 min^{-1}) of nZVI/Pd pariticles. All the results manifested that the coating of SiO_2 greatly improved the reductive activity of the nanoparticles, causing a significant improvement on degradation of BDE47. According to Wan et al.'s results, coating of SiO_2 could effectively reduce the particle surface passivation and severe agglomeration between the particles and enhance the degradation of 2,4-dichlorophenol.[29] The modification of polyvinyl pyrrolidone (PVP) on nZVI/Ni surface was also observed to enhance the aqueous dispersions and catalytic activity to debrominate BDE209.[20]

3.3 Debromination of BDE47 by SiO_2-nZVI/Pd

The debromination of BDE47 was conducted under anoxic conditions with 5 mg L^{-1} (10.28 μM) of initial BDE47 concentration, 1.0 g L^{-1} of SiO_2-nZVI/Pd dosage and 6.00 of pH. Fig.S2 showed the GC-MS chromatographs of BDE47 and the intermediate compounds formed during 120-min debromination. All of PBDEs congeners were identified by matching with the standards (Fig.S3). As shown in Fig.S2, with a decline of BDE47, DE to tri-BDE congeners appeared in a sequential manner, suggesting that BDE47 underwent stepwise debromination to form a series of

congeners during the anaerobic reduction by SiO_2-nZVI/Pd. After 120-min incubation, DE was dominant in the system.

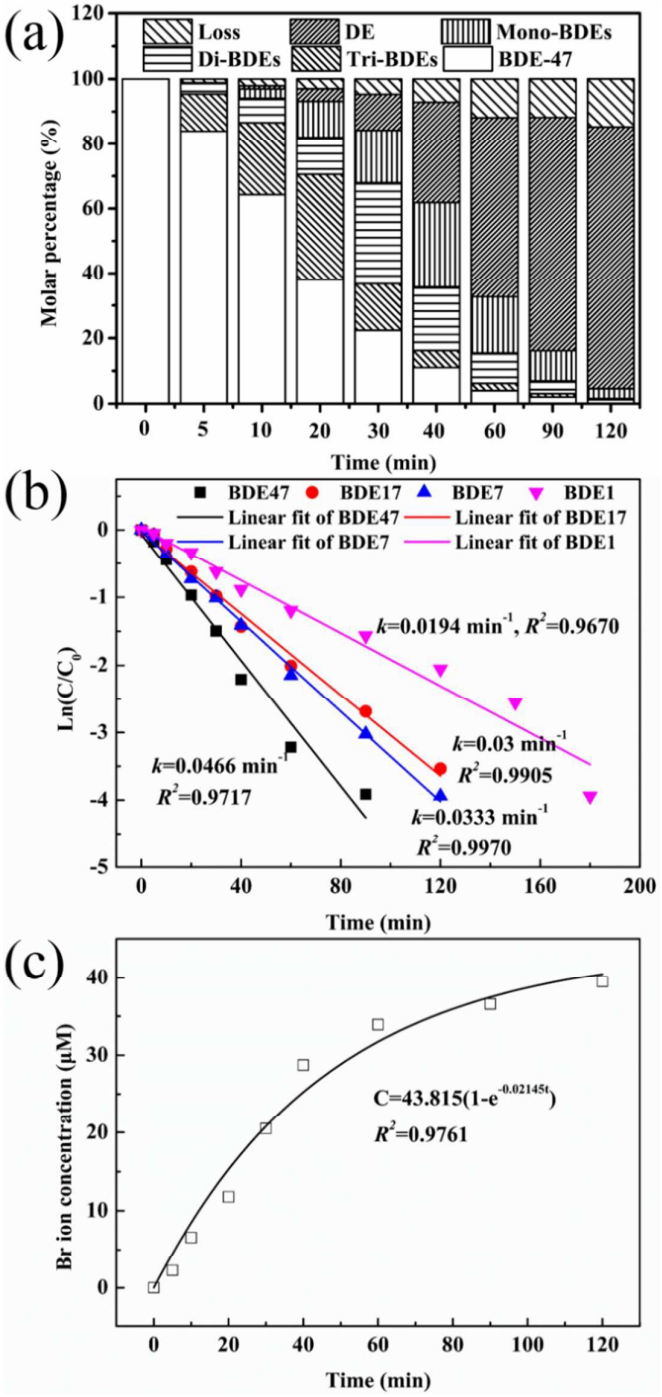

Fig.5 Variation of BDE47 and by-products (a), degradation kinetics of PBDEs (b) and release of Br^- during debromination. SiO_2-nZVI/Pd dosage: 1.0 g L^{-1}, Pd content (wt.%): 0.3%, initial PBDEs concentration: 10.28 μM and initial pH: 6.00.

The variation of BDE47 and by-products and the carbon mass balance were shown in Fig.5. As shown in Fig.5a, BDE47 was almost eliminated in 60 min. Tri-BDEs first appeared in considerable amounts and remained as dominant products in the first 20 min and then declined and finally disappeared after 60 min. From 25 to 35 min, di-BDEs were found to be the main product in the system and almost disappeared after 90 min. The amounts of mono-BDEs increased and reached a peak at 40 min and then faded away in later stages. Meanwhile, with the reaction proceeded, the concentration of DE gradually increased and reached 8.3 μM at the end of anaerobic process. Furthermore, the reductive debromination was intuitively reflected by the release of bromide ion (Fig.5c). The concentration of bromide ion increased continually during the reaction and finally reached 39.5±0.9 μM.

In order to elucidate the rate-limiting step during the complete debromination of BDE47, degradation kinetics of BDE47 and three major products (BDE17, BDE7 and BDE1) were studied under the same condition (Fig.5b). The loss of BDE47 and three main congeners during the debromination reaction were also in accord with the pseudo-first-order model. The rate constants was 0.0466, 0.03, 0.0333 and 0.0194 min^{-1} for BDE47, BDE17, BDE 7 and BDE1, respectively. The relative half-life periods of four congeners was 15.1, 23.1, 20.8 and 35.7 min, indicating that the debromination rate was proportional to the number of bromine on DE. Thus, the debromination of mono-BDE was rate-limiting step during anaerobic reductive process. Interestingly, the rate constant of BDE17 was little lower than that of BDE7, indicating that debromination rate at *ortho* position was lower than that at *para* position. This might be related to the steric hindrance of the bromine atom at the different positions on the benzene ring.[30] The *ortho*-Br endured more hindrance from neighboring oxygen and the neighboring phenyl ring than *para*-Br, leading to the

higher resistance.[19] Meanwhile, the formation of bromide ion (Fig.5c) also followed the first-order kinetic model and its rate constant was 0.0215 min^{-1}. Similar results have been reported in the reductive dechlorination of lindane and TCS by nFe/Pd.[31]

Based on the results above mentioned, it could clear be confirmed that stepwise debromination was the degradation mechanism of BDE47 by SiO_2-nZVI/Pd nanoparticles (Fig.S4). The pathways were similar to those reported for nZVI/Pd,[19,32] demonstrating that SiO_2 had no effects on degradation mechanism of BDE47 by nZVI/Pd. BDE17 and BDE1 were the main products in the debromination pathways for BDE47 and BDE7 resulting from debromination of one *para*-Br, indicating the persistence of *ortho*-Br on the same benzene ring. Furthermore, the appearance of BDE7 followed BDE17 suggested that the debromination preferentially proceeded at the benzene ring with fewer bromine atom. The appearance of BDE28, BDE15 and BDE3 manifested the debromination at *ortho* positions simultaneously occurred, but it was just the minor pathway considering the low amount. Owing to the high reductive activity of nZVI particles, reductive dehalogenation was the main reaction under anaerobic condition, with C-X (X=Cl or Br) bonds sequentially broke and halogen atoms replaced by hydrogen.[5,33]. According to Wang et al.'s study,[33] regioselectivity of the debromination reaction was related to length of the C-Br bonds and an elongation of C-Br bonds was conducive to their rupture. They found that an additional electron from nZVI/Pd combined with the benzene ring and lengthened C-Br bonds at *para* positions, leading to their prior dissociation. Moreover, H atom transfer was found to control PBDE debromination by palladized ZVI.[19,34]. The steric hindrance played a vital role in inhibiting the formation of a precursor complex between the H atom and palladium.[30] The *ortho*-Br bore the most hindrance from neighboring oxygen, while *para*-bromines were least hindered by the oxygen atom and the other phenyl ring,

resulting in a general debromination preference of *para*-Br > *meta*-Br > *ortho*-Br for palladized ZVI.[19]

3.4 Biodegradation of DE by *P. putida* strain

Due the efficient reductive debromination, BDE47 was eventually transformed into non- brominated compound, DE. In this study, an aromatic compounds degrader, *P. putida* strain, was employed for the degradation of DE. For better monitor of TOC and the byproducts during biodegradation, the initial DE was adjusted to 30±2 μM (4.3±0.4 mg L^{-1} of TOC) by adding a measured dose of DE.

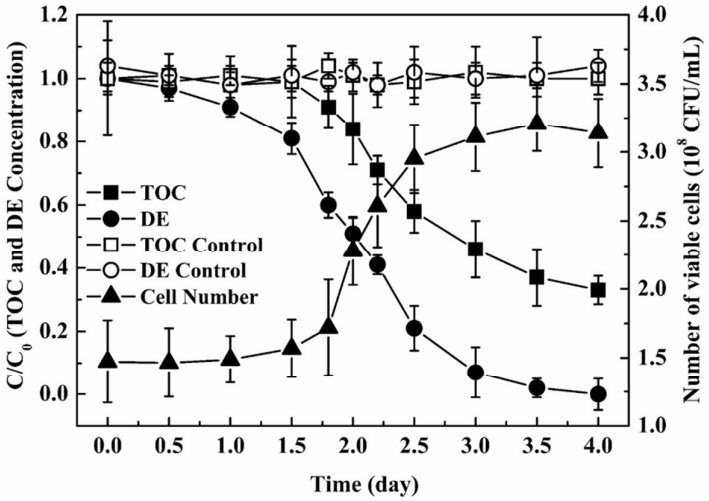

Fig.6 The variation of DE, TOC and viable cell number during the subsequent biodegradation. Initial DE concention: 30±2 μM, initial DE concention: 4.3±0.4 mg L^{-1} and initial pH: 7.00.

During aerobic biodegradation, the variation of DE, TOC and cell number were supervised and the results were shown in Fig.6. As shown in Fig.6, no significant variation of DE and TOC were observed over time in the control experiments, implying that the possible abiotic degradation during the process was basically negligible. However, in the system inoculated *P. putida* cells, the DE was depleted in 3 days, indicating that DE could be rapidly removed by *P. putida* cells. Similarly, the TOC also decreased from 4.3±0.4 to 1.4±0.5 mg L^{-1} after 4 days, suggesting DE and

the intermediates could be easily mineralized by *P. putida* through tricarboxylic acid cycle (TCA). Meanwhile, an evident cell growth (Fig.5) was observed coupled with the DE consumed and the cell number increased to $3.2\pm0.3\times10^{8}$ CFU mL^{-1}, indicating that the substrates could be well utilized for cell growth. According to previous studies,[3,7,8] the PBDEs was rather difficult to be mineralized by the microorganisms even when they were treated for several days or certain months. The great shortening in treating time and improvement in biodegradability were ascribed to the fact that the reduction by SiO_2-nZVI/Pd particles was able to the removal of bromine, hence reducing the resistance and making the products more susceptible to further biodegradation.

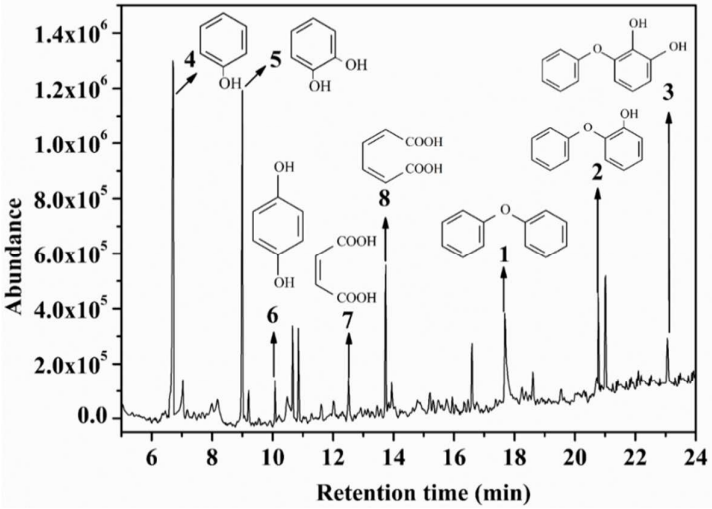

Fig.7 GC/MS analysis of intermediates during biodegradation of DE by *P. putida*.

The *P. putida* strain showed good removal of DE when it was provided as sole source of carbon and energy. However, the degradation pathways of PBDEs by *P. putida* had yet not been reported. To obtain sufficient quantity of intermediates at specific time interval, five bottles were collected and then subjected to triple extraction by dichloromethane. All the extracts were combined and concentrated for the GC-MS analysis of metabolites. The detailed chromatogram and mass spectra of

379 the intermediates at 12 h was presented in Fig.7 and S5. Approximately 7 kinds of
380 possible byproducts were identified through the National Institute of Standards and
381 Technology (NIST11) library and comparison with previous reports.

382 Peak 1 was the target contaminant, DE (RT=17.68 min), with molecular ion at m/z
383 170 and major fragment ions at m/z 141, 77, 51. The peak 2 (RT=20.73) with and 3
384 (RT=23.06) which gave molecular ion at m/z 186 and 202 were identified as mono-
385 hydroxylated and di-hydroxylated DE products, respectively. Peak 2 was confirmed as
386 2-hydroxy DE (major fragment ions at m/z 158, 109, 77), but the specific structure of
387 peak 3 could not be fully confirmed with certainty through NIST11. According to
388 Yamazoe et al.'s results,[35] 2,3-dioxygenation was a common enzyme during the
389 metabolic process of *P. putida* strain, which could add a hydroxyl group at the
390 2,3-positions of the benzene ring. Thus, peak 3 was speculated to be
391 2,3-dihydroxydiphenol ether. The peaks (4-6) with retention time at 6.70, 9.21 and
392 10.07 min were a series of phenolic compounds formed via the cleavage of ether bond,
393 which were identified as phenol, catechol and *p*-hydroquinone, respectively. The peak
394 7 (RT=12.51 min) and 8 (RT=13.72 min) with molecular ion at m/z 116 and 142 were
395 ring-opening products, which were maleic acid and trans,trans-2,4-hexadienedioic
396 acid, respectively.

397 According to Bressler and Fedorak's results,[36] aerobic biodegradation of polycyclic
398 aromatic compounds by bacteria was a process which involved a complex
399 oxygenation enzyme system. Generally, oxygenation systems are divided into three
400 different types: (a) lateral dioxygenation, in which one of the aromatic rings is
401 hydroxylated; (b) angular dioxygenation, in which the carbon atom bonded to the
402 heteroatom and the adjacent carbon in the aromatic ring are both oxidized to
403 hemiacetal; and (c) five-membered ring monooxygenation, in which the methylene

carbon atom is oxidized. Based on the identified intermediates, a degradation pathway of DE by *P. putida* strain was proposed in Fig.8. In this study, both lateral dioxygenation and angular dioxygenation occurred during the biodegradation of DE by *P. putida*in. The formation of 2,3-dihydroxydiphenol ether suggested that lateral dioxygenation occurred at 2,3'-positions of benzene ring. Due to the dehydration, 2,3-dihydroxydiphenol ether would transform into 2-hydroxydiphenyl ether.[3532] Meanwhile, Identification of several phenolic compounds, such as phenol, catechol and hydroquinone confirmed that the angular dioxygenation simultaneously occurred to DE and 2-hydroxydiphenyl ether during the biodegradation, which led to cleavage of ether bond. Subsequently, further oxidization and ring cleavage resulted in generation of a series of carboxylic acids like maleic acid and trans,trans-2,4-hexadienedioic acid. Finally, the carboxylic acids were mineralized into CO_2 and H_2O via the tricarboxylic acid cycle (TCA). Similarly, both angular dioxygenation and lateral dioxygenation were verified in the degradation of diphenyl ether by *Janibacter sp*. strain YY-1[35] and *bacillus cereus* JP12.[8] In previous study, the angular dioxygenation was mostly confirmed during the biodegradation of PBDEs by *sphingomonas sp*..[9,37,38] Meanwhile, Pfeifer et al.[39] found that lateral dioxygenation occurred when the *Pseudomonas cepacia* Et4 was employed for the degradation of DE. However, lateral dioxygenation pathway would result in the formation of some toxic products such as dibenzo-p-dioxins, dioxin and hydroxylated PBDEs.[8,35] To the best of our knowledge, there is little information in the literature on the PBDEs degradation pathway by *Pseudomonas putida* strain. In this study, PBDEs degradation pathway utilized by this strain was similar to the pathway reported for *Janibacter sp*. strain and *bacillus cereus* JP12.

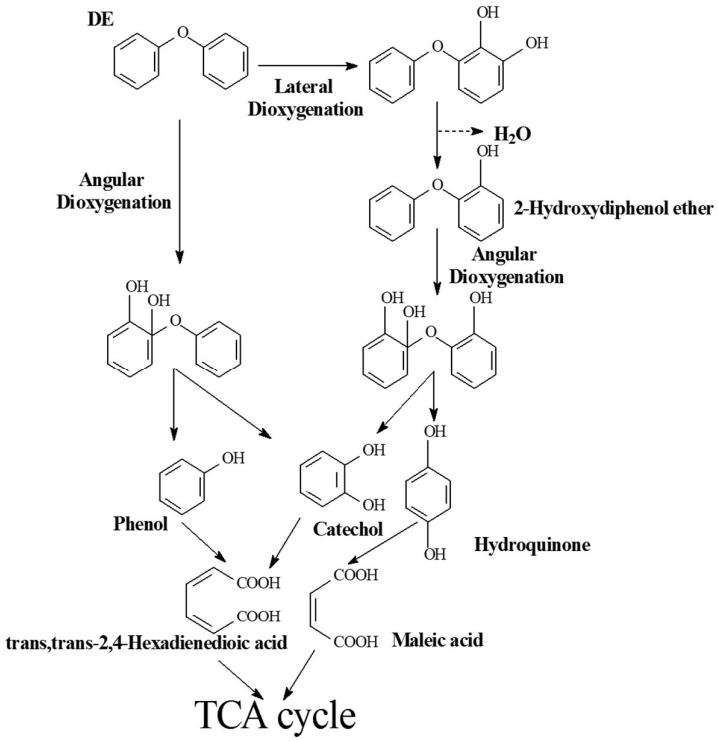

Fig.8 Aerobic degradation mechanism of DE by *P. putida* strain.

4 Conclusions

The results of this study indicated that SiO_2-nZVI/Pd was a promising pretreatment process for remediation of PBDEs particularly when employed in combination with biological treatment.

(1) Compared with nZVI/Pd, SiO_2-nZVI/Pd particles exhibited much lower toxicity to the growth of *P. putida* strain and higher reactivity on reductive debromination.

(2) During the pretreatment by SiO_2-nZVI/Pd, BDE47 could be completely transformed into DE through step-by-step debromination, reducing the toxicity and resistance of the products. This made the treated effluent compatible for further biological treatment whilst avoiding the formation of highly toxic intermediates such as bromphenols and OH-PBDEs.

(3) After debromination, DE could be fully utilized and mineralized by *P. putida* strain and 67% of TOC was removed after 4 days of aerobic biodegradation.

The results indicated that SiO_2-nZVI/Pd-microorganisms combined process could be a potential strategy for complete remediation of refractory POPs such as PCB and PBDEs, especially in the highly polluted districts.

Acknowledgements

The research was financially supported by grants from Guangdong Province Science and Technology Project (No: 2013B090200016, 2013B021000008, 2015B020215007, 2015B020235009), Joint fund of Guangdong Province (NO: U1401235) and Major Science and Technology Program for the Industry-Academia-Research Collaborative Innovation of Guangzhou.

References

1. S. Wang, S. Zhang, H. Huang and P. Christie, *Environ. Pollut.*, 2011, **159(3)**, 749.
2. P. Wang, Q. Zhang, T. Wang, W. Chen, D. Ren, Y. Li and G. Jiang, *Rsc Adv.*, 2012, **2(4)**, 1350.
3. K. R. Robrock, P. Korytár and L. Alvarez-Cohen, *Environ. Sci. Technol.*, 2008, **42(8)**, 2845.
4. L. Jing, Y. E. Shi, J. Cui, X. Zhang and J. Zhan, *RSC Adv.*, 2015, **5(18)**, 13443.
5. Y. S. Keum and Q. X. Li, *Environ. Sci. Technol.*, 2005, **39**, 2280.
6. V. Richardson, D. Staskal, D. Ross, J. Diliberto, M. DeVito and L. Birnbaum, *Toxicol. Appl. Pharm.*, 2008, **226**, 244.
7. G. Shi, H. Yin, J. Ye, H. Peng, J. Li and C. Luo, *Chemosphere*, 2013, **93(8)**, 1487.
8. M. Lu, Z.Z. Zhang, X.J. Wu, Y.X. Xu, X.L. Su, M. Zhang and J.X. Wang, *Bioresour. Technol.*, 2013, **149**, 8.
9. Y.M. Kim, I.H. Nam, K. Murugesan, S. Schmidt, D.E. Crowley and Y.S. Chang,

Appl. Microbiol. Biot., 2007, **77(1)**, 187.

10. A. Malmvärn, Y. Zebühr, L. Kautsky, Å. Bergman and L. Asplund, *Chemosphere*, 2008, **72(6)**, 910.
11. S. R. Kanel, B. Manning, L. Charlet and H. Choi, *Environ. Sci. Technol.*, 2005, **39(5)**, 1291.
12. A. B. Giasuddin, S. R. Kanel and H. Choi, *Environ. Sci. Technol.*, 2007, **41(6)**, 2022.
13. K. Murugesan, V. Bokare, J. R. Jeon, E. J. Kim, J. H. Kim and Y. S. Chang, *Bioresour. Technol.*, 2011, **102(10)**, 6019.
14. X. Chen, G. Chen, M. Qiu, G. Sun, J. Guo and M. Xu, *Environ. Sci. and Pollut. R.*, 2014, 21(13), 7856.
15. N. He, P. J. Li, Y. C. Zhou, W. X. Ren, S. X. Fan and V. A. Verkhozina, *J. Hazard. Mater.*, 2009, **164**, 126.
16. Y. M. Kim, K. Murugesan, Y. Y. Chang, E. J. Kim and Y. S. Chang, *J. Chem. Technol. Biot.*, 2012, **87(2)**, 216.
17. Y. H. Shih, H. L. Chou, Y. H. Peng and C. Y. Chang, *Bioresour. Technol.*, 2012, **108**, 14.
18. S. Xia, Z. Gu, Z. Zhang, J. Zhang and S. W. Hermanowicz, *Chem. Eng. J.*, 2014, **257**, 98.
19. Y. Zhuang, S. Ahn, A. L. Seyfferth, Y. Masue-Slowey, S. Fendorf and R. G. Luthy, *Environ. Sci. Technol.*, 2011, **45**, 4896.
20. Z. Fang, X. Qiu, J. Chen and X. Qiu, *J. Hazard. Mater.*, 2011, **185(2)**, 958.
21. C. H. Lee, J. Y. Kim, W. I. Lee, K. Nelson, J. Y. Yoon and D. Sedlak, *Environ. Sci. Technol.*, 2008, **42**, 4927.
22. M. H. Diao and M. S. Yao, *Water Res.*, 2009, **43**, 5243.

23. J. Y. Kim, H. J. Park, C. Lee, K .L. Nelson, D. L. Sedlak and J. Yoon, *Appl. Environ. Microbiol*., 2010, **76**, 7668.
24. Z. Li, K. Greden, P. J. J. Alvarez, K. B. Gregory, G. V. Lowry, *Environ. Sci. Technol.*, 2010, **44**, 3462.
25. Y. An, T. Li, Z. Jin, M. Dong, H. Xia and X. Wang, *Bioresour. Technol.*, 2010, **101**, 9825.
26. Y. C. Lv, Y. C. Chen, S. Y. Sun and Y. Y. Hu, *Bioresour. Technol.*, 2014, **155**, 144.
27. G. V. Lowry and Johnson, K. M, *Environ. Sci. Technol.*, 2004, **38(19)**, 5208.
28. J. L. Sebaugh, *Pharm. Stat.*, 2011, **10(2)**, 128.
29. J. Wan, J. Wan, Y. Ma, M. Huang, Y. Wang and R. Ren, *Chem. Eng. J.*, 2013, **221**, 300.
30. Y. Noma, M. Ohno and S. *Sakai, Fresen. Environ. Bull.*, 2003, **12**, 302.
31. V. Nagpal, A. D. Bokare, R. C. Chikate, C. V. Rode and K. M. Paknikar, *J. Hazard. Mater.*, 2010, **175**, 680.
32. Y. Zhuang, L. Jin and R. G. Luthy, *Chemosphere*, 2012, **89(4)**, 426.
33. S. Wang, C. Hao, Z. Gao, J. Chen, J. Qiu, *Chemosphere*, 2012, **88**, 33.
34. J. Kim, P. G. Tratnyek and Y. Chang, *Environ. Sci. Technol.*, 2008, **42(11)**, 4106.
35. A. Yamazoe, Y. agiO. and H. Oyaizu, *Biotechnol. Lett.*, 2004, **26(6)**, 479.
36. D. C. Bressler and P. M. Fedorak, *Can. J. Microbiol.*, 2000, **46**, 397.
37. S. Schmidt, R. Wittich, D. Erdmann, H. Wilkes, W. Francke and P. Fortnagel, *Appl. Environ. Microbiol.*, 1992, **58**, 2744.
38. S. Schmidt, P. Fortnagel and R. Wittich, *Appl. Environ. Microbiol.*, 1993, **59**, 3931.
39. F. Pfeifer, S. Schaht, J. Klein and H. G. Truper, *Arch. Microbiol.*, 1989, **152**, 515.

518 **Figure Captions**

519 Fig.1 TEM images (a-d) and size distribution (e) of SiO_2-nZVI/Pd and XRD (f)
520 spectra of SiO_2-nZVI/Pd, nZVI/Pd, nZVI, Pd and SiO_2.

521 Fig.2 Effect of nZVI/Pd and SiO_2-nZVI/Pd nanoparticles on the growth (a) and
522 inactivation (b) of *P. putida* in MSM medium. Initial cell concentration:
523 $2.0\pm0.6\times10^7$ CFU mL^{-1} and initial pH: 7.00.

524 Fig.3 TEM images of *P. putida* cells (a), nZVI/Pd treated cells (b) and SiO_2-nZVI/Pd
525 treated cells (c) and the biological slices of *P. putida* cells (d) and nZVI/Pd treated
526 cells (e). Initial cell concentration: $2.0\pm0.6\times10^7$ CFU mL^{-1}, nZVI/Pd dosage: 0.5 g
527 L^{-1} and SiO_2-nZVI/Pd dosage: 1.0 g L^{-1}.

528 Fig.4 Effects of particle dosage on degradation of BDE47.

529 Fig.5 Variation of BDE47 and by-products (a), degradation kinetics of PBDEs (b) and
530 release of Br^- during debromination. SiO_2-nZVI/Pd dosage: 1.0 g L^{-1}, Pd content
531 (wt.%): 0.3%, initial PBDEs concentration: 10.28 μM and initial pH: 6.00.

532 Fig.6 The variation of DE, TOC and viable cell number during the subsequent
533 biodegradation. Initial DE concention: 30±2 μM, initial DE concention: 4.3±0.4 mg
534 L^{-1} and initial pH: 7.00.

535 Fig.7 GC/MS analysis of intermediates during biodegradation of DE by *P. putida*
536 strain.

537 Fig.8 Aerobic degradation mechanism of DE by *P. putida* strain.
538

Graphical Abstract